Validation of VSPAERO for Basic Wing Simulation

Jose Rosas-Cordova[1], Carlos Santana-Delgado[1,*], Diana Hernandez-Alcantara[2] and Luis Amezquita-Brooks[1,*]

[1] Facultad de Ingeniería Mecánica y Eléctrica, Universidad Autónoma de Nuevo León, San Nicolás de los Garza, 66455, Mexico

[2] Escuela de Ingeniería y Tecnologías, Universidad de Monterrey, San Pedro Garza García, 66238, Mexico

INFORMATION

Keywords:
Wing simulation
potential flow solver
vortex-lattice method
OpenVSP

DOI: 10.23967/j.rimni.2024.10.056492

Revista Internacional de Métodos Numéricos para Cálculo y Diseño en Ingeniería

Validation of VSPAERO for Basic Wing Simulation

Jose Rosas-Cordova[1], **Carlos Santana-Delgado**[1,*], **Diana Hernandez-Alcantara**[2] and **Luis Amezquita-Brooks**[1,*]

[1]Facultad de Ingeniería Mecánica y Eléctrica, Universidad Autónoma de Nuevo León, San Nicolás de los Garza, 66455, Mexico

[2]Escuela de Ingeniería y Tecnologías, Universidad de Monterrey, San Pedro Garza García, 66238, Mexico

ABSTRACT

Potential flow theory-based numerical solvers have gained popularity for rapid and straightforward aerodynamic modeling across various applications, particularly in the early stages of design and in resource-limited projects such as small unmanned aerial vehicles (UAVs). These solvers offer a cost-effective solution for analyzing aerodynamic performance, and several well-established methods have demonstrated strong alignment with experimental data. Among these solvers is VSPAERO, a relatively recent addition integrated within the National Aeronautics and Space Administration's (NASA) OpenVSP aircraft design software. Despite its growing use, a comprehensive validation of the VSPAERO solver remains necessary to ensure its reliability in diverse scenarios. This article presents a validation of the VSPAERO solver by conducting a series of case studies. The assessment includes comparisons against reference values obtained through empirical relationships, results from other established aerodynamic solvers and experimental data from wind tunnel testing. The assessment covers a range of geometries and flow conditions, highlighting areas where the solver performs well and identifying any limitations in its application. The findings provide insights into the meshing parameters required for accurate simulations, as well as the types of geometries and flow conditions for which VSPAERO can be considered a reliable tool. As a conclusion, the article presents a series of best practices and guidelines that are recommended to improve the accuracy and efficiency of future aerodynamic simulations conducted using this software. These recommendations are intended to serve as a valuable reference for both researchers and engineers involved in aerodynamic modeling, particularly those working on projects with tight budgets or in the preliminary stages of aircraft design.

OPEN ACCESS

Received: 24/07/2024

Accepted: 18/09/2024

DOI
10.23967/j.rimni.2024.10.056492

Keywords:
Wing simulation
potential flow solver
vortex-lattice method
OpenVSP

Glossary/Nomenclature/Abbreviations

AR	Aspect ratio

*Correspondence: Carlos Santana-Delgado, Luis Amezquita-Brooks (csantanad@uanl.edu.mx, luis.amezquitabrk@uanl.edu.mx).

TR	Taper ratio
b	Wingspan
C_{Di}	Induced drag coefficient
C_L	Three-dimensional lift coefficient
C_M	Pitching moment coefficient
c_L	Two-dimensional lift coefficient
c	Chord
Ma	Mach number
Re	Reynolds number
x_{CG}	Pitching moment reference point
y	Span-wise coordinate
α	Angle of attack
$\Lambda_{c/2}$	Mid-chord sweep
λ	Taper ratio
ϕ_G	Geometric twist

Subscripts

0	Value at zero angle of attack
ref	Reference value
α	Derivative wrt. the angle of attack

1 Introduction

The ability to predict the aerodynamic characteristics of an aircraft during all phases of its development is essential to ensure the creation of a vehicle capable of meeting mission-specific requirements. Accurate predictions early in the design process help guide crucial decisions, ultimately leading to a more efficient and reliable aircraft. Potential flow theory, commonly used in solvers based on lifting-line, vortex-lattice, and panel methods, has gained increasing popularity due to its low computational cost and ease of use. These features make potential flow solvers particularly attractive during the conceptual and preliminary design phases when computational resources are often limited, and rapid iteration is required.

Software packages such as XFLR5 and Athena Vortex Lattice (AVL) enhance potential flow solvers by providing user-friendly interfaces that simplify design and analysis tasks. However, despite their widespread use, validation studies for these solvers remain relatively scarce in the literature. Nonetheless, the available reports generally indicate good agreement between the results from these solvers and experimental data, especially for linear solvers like XFLR5, AVL, PMARC, and LSAERO. Such tools are often applied in the design of small aircraft, particularly in academic settings [1–4]. For instance, in [1], XFLR5 was used together with sub-parametric finite-element parametrization to determine the basic aerodynamic properties of airfoils under low Reynolds number flow conditions. In [2], legacy AVL code written in FORTRAN was integrated into a modern programming environment, allowing the solver to be applied to contemporary conceptual design problems. These examples illustrate the continuing relevance and applicability of potential flow solvers in various stages of the aircraft design process.

Other studies have undertaken comparisons between potential flow solvers and more complex computational fluid dynamics (CFD) methods. For example, in [3], the performance of several Navier-Stokes, potential flow, empirical methods, and handbook formulas was compared, revealing that

potential flow solvers offer a favorable balance between computational complexity, user-friendliness, and accuracy. These findings underscore the value of potential flow solvers in cases where computational efficiency is essential, particularly in early-stage design or for small-scale projects. The lower computational cost of these solvers makes them an attractive option, especially in the design of small UAVs or academic research contexts where computational resources are limited.

In this context, VSPAERO stands out as a linear aerodynamic solver embedded within NASA's OpenVSP aircraft design software [5]. VSPAERO offers both vortex-lattice and panel methods, making it more versatile compared to other solvers like XFLR5, AVL, PMARC, and LSAERO. One of the key advantages of VSPAERO is its ability to predict the aerodynamic performance of a modeled geometry directly within OpenVSP, without the need for exporting or remodeling the vehicle in other software platforms. This feature significantly streamlines the design process, enabling rapid iterations and reducing potential errors during geometry transfer. Additionally, VSPAERO provides interfaces for Python and MATLAB, facilitating the automation of design optimization tasks and increasing its usability in more complex workflows. These features make VSPAERO a highly attractive option for conceptual and preliminary aircraft design, particularly when ease of integration with optimization frameworks is desired. Some of the analysis tasks that can be accomplished using this tool are described in [6]. These low cost but effective tools are an attractive alternative for aerodynamic [7,8] and stability analyses [9,10] for small scale autonomous aircraft.

Due to their efficiency, these solvers have been integrated into more complex optimization algorithms, such as genetic and meta-heuristic methods, to address multi-objective design problems. For instance, in [11], AVL was integrated within a double-loop optimization algorithm to generate optimal conceptual designs based on objectives like maximum reliability and minimum takeoff weight. In another example [12], AVL and XFLR5 were utilized to solve a comprehensive multi-objective design problem that considered factors such as takeoff weight, required power, endurance, and lift and drag coefficients. These studies underscore the importance of lightweight solvers in optimization scenarios where multiple simulations are necessary to converge on an optimal design.

Despite the growing use of VSPAERO, particularly in small aircraft design, there is a relative scarcity of published validation studies, largely due to the solver's relative novelty. Two notable exceptions include [13,14], which provide early efforts at validating the solver's performance. These studies are crucial for building confidence in VSPAERO as a reliable tool for aerodynamic analysis. The absence of extensive validation studies suggests a need for further exploration to fully understand the solver's capabilities and limitations.

In light of this, the present article aims to contribute to the validation of VSPAERO by focusing on its vortex-lattice method solver. A series of validation studies are conducted, comparing VSPAERO's performance with reference data obtained from analytical methods, handbooks, and experimental measurements. The selected case studies include both classical aerodynamic problems and recent experimental data, allowing for a comprehensive assessment of the solver's accuracy. The first five cases presented in this article are based on the results from [15], while the last two cases are taken from [16], incorporating experimental data to further validate the solver.

The comparison with reference data presented here can provide valuable insights into the accuracy and reliability of the solver in different scenarios. The findings of this study can be particularly useful for researchers and engineers involved in aerodynamic design at the conceptual stage.

2 Validation Case Studies

A selection of wing planforms was made for this article. This selection aims at covering the main variables and conditions which can be of importance for the application area. Namely, sweep, taper and aspect ratio variations, as well as low Re operating conditions. In addition, the availability of data for each wing in the literature was also taken into consideration.

Before starting with the different case studies, a set of basic meshing parameters, mainly the clustering values, had to be established. These parameters control the spacing between consecutive mesh slices and were based on the results and recommendations given in [14]. The settings using along all the simulations of the article were: 0.25, 0.25, 1.0 and 0.5 for the leading edge, trailing edge, the root and the tip clusters, respectively.

A summary of all the wing planforms considered along the article is shown in Fig. 1. Further details including tables describing the planform geometries for each analysis and images of the developed OpenVSP models can be found on the Appendix A at the end of the article. In addition, during the development of the article, heavy use of the OpenVSP AngelScript and Python APIs allowed for the automation of all case studies (all the employed code will is freely available in the GitHub repository https://github.com/JARC99/vspaero-validation-studies, accessed on 17 September 2024).

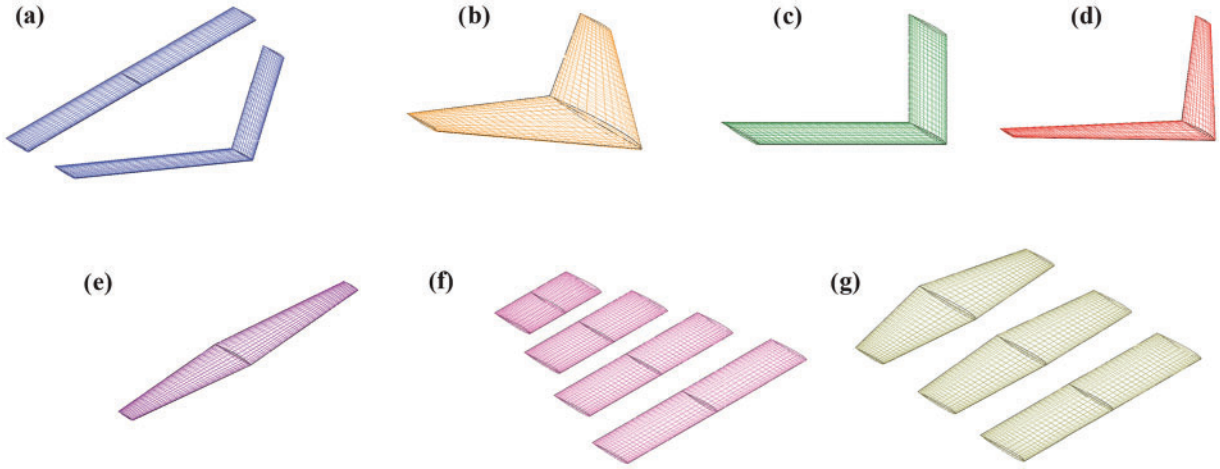

Figure 1: Wing planforms used along the article. (a) Straight and swept wings comparison, (b) Warren-12 wing, (c) Bertin-Smith 2D wing, (d) NACA R-1208 tapered and swept wing, (e) NACA TN-1422 straight tapered wing, (f) low Re aspect ratio comparison, (g) low Re taper comparison

2.1 3D Properties of Two Wings

The first set of analyses was centered around determining which combination of chord and span-wise mesh resolution should be used to obtain acceptable results within a reasonable execution time.

The flow around two wings differing only in leading edge sweep (Fig. 1a) was simulated at an angle of attack (AOA) of 10°. The details of these wings are presented in Fig. A1 and Table A1. From these simulations the main wing parameters, i.e., the lift curve slope, lift, and induced drag coefficients were obtained. In order to single out the effects of varying the mesh in each direction, the tessellation value was modified first along the chord-wise direction while maintaining the span-wise resolution in the default value of 6; afterwards, the span-wise tessellation was varied while the chord-wise value was kept constant at the default value of 33.

The results obtained by carrying out the previously described analyses are presented in Fig. 2. This figure shows the VSPAERO data points alongside the results given by the SURFACES vortex-lattice solver reported in [15]. In addition, a reference value, obtained from the empirical relationships given in the USAF DATCOM algorithms, is also included in each figure, together with a ±5% band represented as a shaded band (i.e., values inside the shaded area are within ±5% of the USAF DATCOM reports).

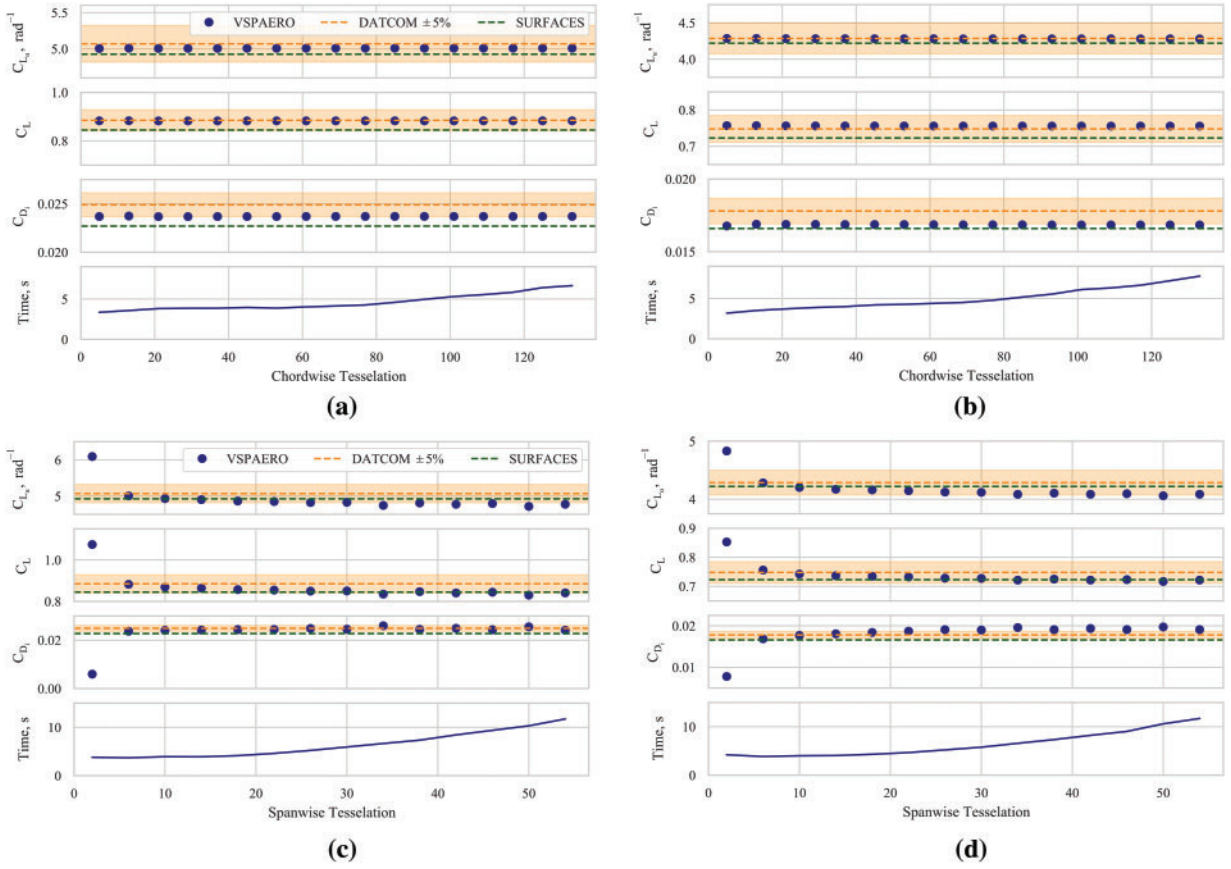

Figure 2: Main wing parameters obtained by modifying the wing chord-wise (a, b) and span-wise (c, d) tessellation value for both wing configurations: (a) 0° and (b) 35°. The shaded area represents a ±5% band from the *reference value*

The derivation of the reference values is presented in full detail in [15]; however, for convenience, the required formulas are summarized next:

$$C_{L_\alpha} = \frac{2\pi \cdot AR}{2 + \sqrt{\left(\frac{AR \cdot c_{L_\alpha}}{2\pi}\right)^2 \left(1 + \frac{\tan \Lambda_{c/2}{}^2}{1 - Ma^2}\right) + 4}}, \tag{1}$$

$$C_{D_i} = \frac{C_L^2}{\pi \cdot AR}, \tag{2}$$

$$C_{L_0} = 0. \tag{3}$$

Fig. 2a,b shows that the chord-wise tessellation has a negligible effect on the obtained results. In fact, although the studied range was considerably large, the percent difference between the highest and lowest tessellation settings averages 0.030% for all parameters. In a similar manner, the solution times of the coarsest and finest mesh are practically the same. Nonetheless, a more noticeable uptrend is appreciable on the swept wing.

On the other hand, from Fig. 2c,d, it can be seen that the increase of the span-wise tessellation has a more noticeable effect on both the accuracy of the results as well as the simulation execution time. Starting from the minimum allowable tessellation value of 2, the coefficient values converge rather quickly. In particular, for the straight wing any tessellation value after the second point, around the 4 mark, results in a convergent estimation. In contrast the swept wing needs a significantly finer mesh to be able to yield consistent results. The use of an excessively refined mesh along the span-wise direction is limited by the fact that above a value of 30 the simulation times start to increase significantly. Nonetheless, these simulation times are still much lower than that of other computer fluid dynamics approaches.

Overall, Fig. 2 shows that chordwise tessellation requires to be set at 4, while spanwise tessellation requires at least 10, for convergence. In the other hand, increasing chord and span-wise tessellation values over 30 and 20 respectively did not provided further improvements, while it increased simulation time. Considering this, along the article chord and span-wise tessellation values of 33 and 24 are used since they ensure a good level of convergence with a reasonable computational time using the VSPAERO solver.

Finally, Table 1 shows a quantitative summary using these tessellation settings in comparison with the reference values for the two studied wing geometries.

Table 1: Comparison of the VSPAERO and DATCOM reference results for both wings with chord and span-wise tessellation values of 33 and 24, respectively

	Wing 1			Wing 2		
Coefficient	DATCOM	VSPAERO	Error, %	DATCOM	VSPAERO	Error, %
C_{L_α}, rad^{-1}	5.071	4.824	4.81	4.286	4.108	4.10
C_L	0.885	0.851	3.89	0.748	0.726	2.92
C_{D_i}	0.0249	0.0239	3.85	0.0178	0.0185	4.03

2.2 Warren-12 Wing

The Warren-12 wing model, shown in (Fig. 1b), is a standard case study used for the validation of new or modified VLM codes [15]. The details of the Warren-12 wing are presented in Fig. A2 and Table A2. As mentioned in the previous section, the wing tessellation was set to 33 and 24 for the chord- and span-wise directions, respectively. An AOA sweep from 0° to 10° was simulated with VSPAERO. Fig. 3 shows the resulting lift a pitching moment coefficient plots together with the reference values reported in [15].

The agreement between the three curves shown in Fig. 3 is remarkable, albeit expected because of method similarities. Table 2 summarizes the resulting coefficient derivatives as well as the average percent error of all the calculated points with respect to the reference values reported in [15] and those

obtained using SURFACES. Similarly to the previous results, the average percent error does not exceed the 5% mark.

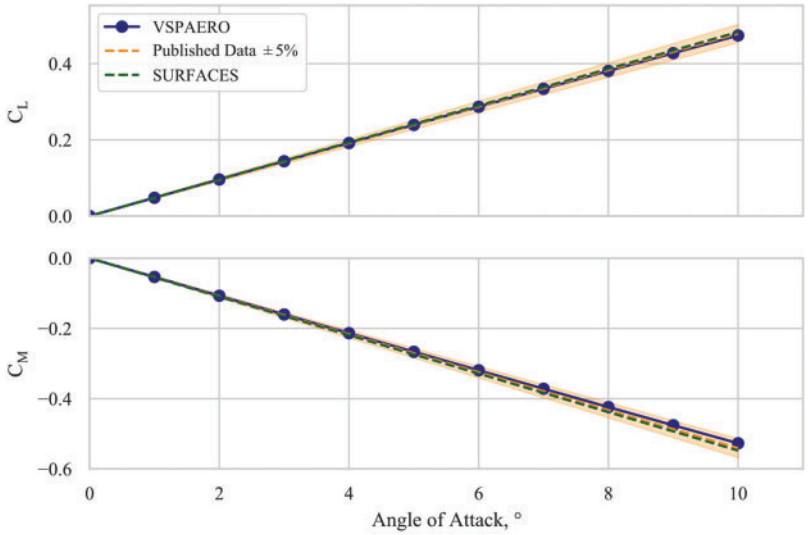

Figure 3: Calculated and reference lift and pitching moment coefficient curves of the Warren-12 wing

Table 2: Comparison of the VSPAERO, SURFACES, Tornado with literature reference values for well-known wings planforms

			VSPAERO		SURFACES		Tornado	
Wing	Coefficient	Reference	Value	Error, %	Value	Error, %	Value	Error, %
Warren	C_{L_α}, rad^{-1}	2.715	2.743	1.01	2.767	1.92	–	–
Bertin	C_{M_α}, rad^{-1}	−3.020	−3.10	2.56	−3.139	3.94	–	–
	C_{L_α}, rad^{-1}	3.433	3.194	6.96	3.442	0.26	3.450	0.50

2.3 Bertin-Smith 2D Wing

Similarly to the previous case study, the Bertin-Smith 2D wing (Fig. 1c) can be used as a theoretical benchmark to validate the numerical results of a VLM solver. The wing is given out as an exercise in [17] and a series of calculations are carried out to determine the value of the lift curve slope. The details of this wing are presented in Fig. A3 and Table A3.

Analogous to the procedure followed in section dealing with the Warren-12 wing, the chord- and span-wise tessellations were set to 33 and 24, respectively. A sweep analysis from 0° to 10° was carried out in VSPAERO resulting in the curve shown in Fig. 4. Alongside the lift curve calculated with VSPAERO, the plot also includes the reference slope reported in [17] and two other curves computed using two alternative VLM solvers: SURFACES and Tornado [15]. Table 2 summarizes the obtained results for the three solvers.

In this case, the results obtained with VSPAERO present a greater deviation from those obtained using the other solvers. The tendency of the solver to under-predict the value of the lift curve slope

can be also observed in a previous case study in Fig. 2. Overall, in this case the deviation amounts to approximately 7% from the reference value. Although greater that in the previous cases, this error level may still be acceptable for many applications in the early stages of the design process.

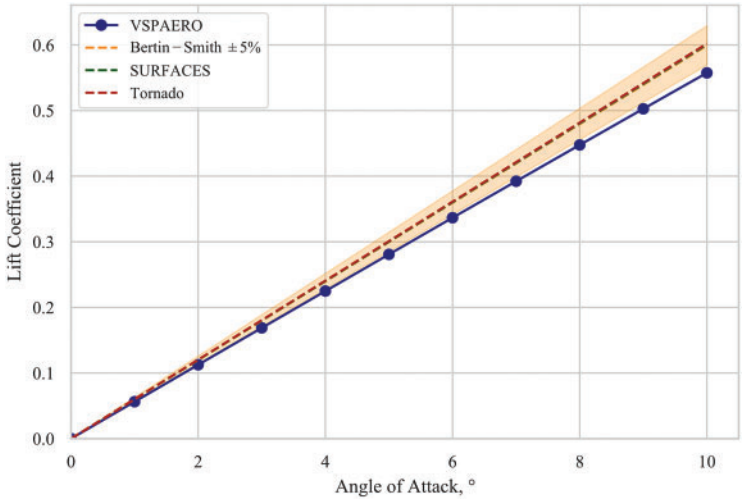

Figure 4: Lift curve for the Bertin-Smith wing calculated with different methods (the results obtained with SURFACES and Tornado match the reference results almost exactly)

2.4 NACA R-1208

In this case-study, experimental data is incorporated for the accuracy assessment of VSPAERO. Specifically, the wind-tunnel measurements reported in [18] are used, which have also been recently used for simulation validation in [19]. Similarly to previous cases, the wing geometry is a swept-back wing of moderate aspect ratio shown in Fig. 1d. Further details of this wing are presented in Fig. A4 and Table A4.

The two following analyses were carried out:

1. An AOA sweep from 0° to 10° to calculate the lift and pitching moment coefficient curves of the wing.

2. A load distribution analysis at a fixed AOA of 4.7° to obtain the normalized lift coefficient distribution along the span of the wing.

The resulting lift and pitching moment curve plots are shown in Fig. 5. The lift curve shows good agreement with the experimental values throughout the linear range. On the other hand, the calculated moment coefficient values on the second half of the studied range deviate significantly from the expected experimental values even withing the linear lift range. This can be attributed to the highly non-linear behavior observed in the experimental data, which can be explained with the early tip stall phenomena characteristic of swept back wings, a phenomenon difficult to predict for an inviscid solver. A similar deviation was observed in [15] with the SURFACES VLM solver. In the case of the local lift coefficient distribution (shown in Fig. 5c), the results computed using VSPAERO show close agreement to the reported experimental values. Table 3 summarizes the results.

2.5 NACA TN-1422

This case study also includes experimental data and is based in the wind-tunnel test results reported in [20] for two wing configurations differing only in the washout angle (0° and 2°), which has also been used for simulation validation recently [21]. Both wings are based on a straight tapered planform of moderate aspect ratio shown in Fig. 1e. Further details of this wing are presented in Fig. A5 and Table A5.

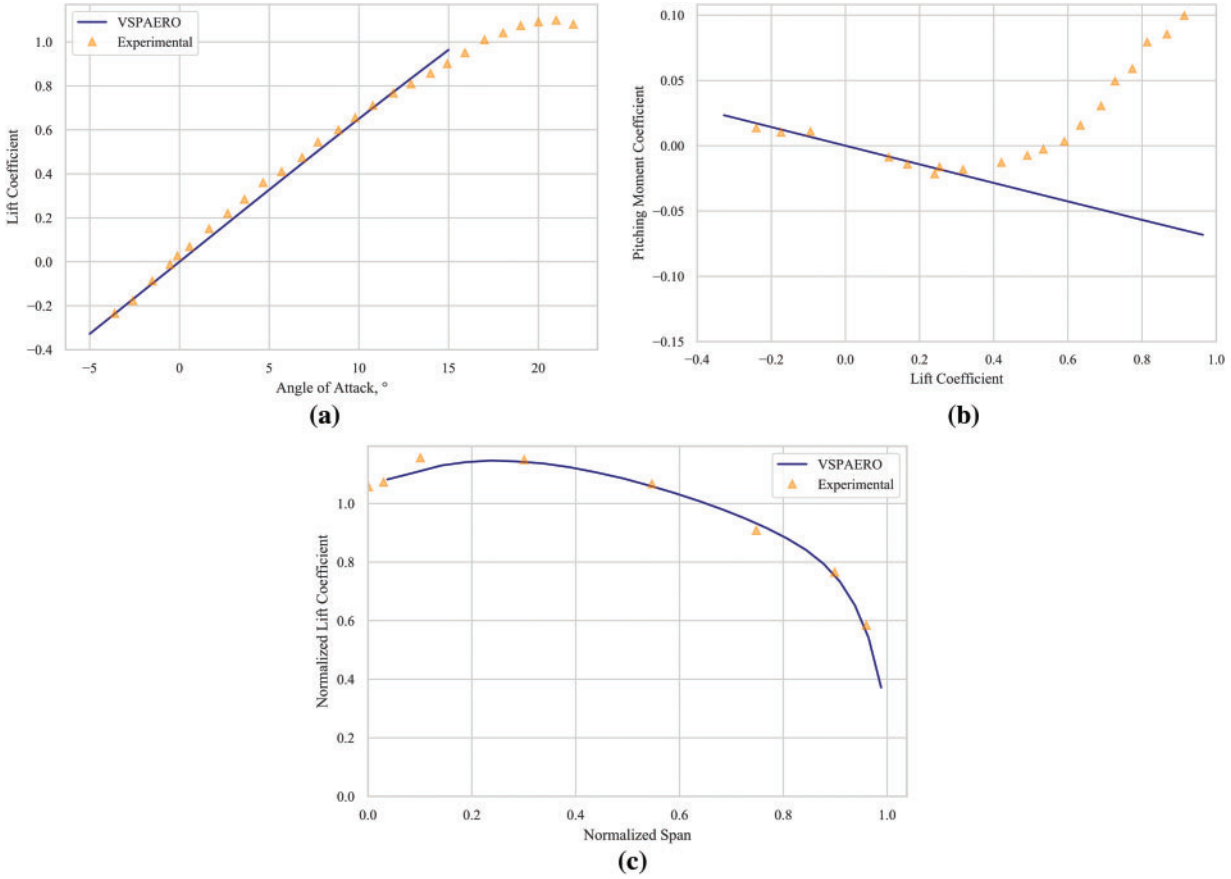

Figure 5: Resulting (a) lift coefficient, (b) pitching moment coefficient, and (c) normalized span-wise lift coefficient distribution curves plotted against the experimentally obtained data points

Table 3: Comparison between VSPAERO and the experimentally obtained results reported in [18]

Coefficient	R-1208	VSPAERO	Error, %
C_{L_α}, rad^{-1}	3.493	3.700	5.91
$\frac{dC_{M_l}}{dC_L}$	−0.0727	−0.0714	1.59
$c_L = f\left(\frac{2y}{b}\right)$	—	—	2.50

Note: [1]Before tip stall where the C_M values diverge due to nonlinearities in the flow condition (i.e., $C_L > 0.4$).

Analogous to the previous section, VSPAERO was employed to carry out an AOA sweep as well as a span-wise lift coefficient distribution. The resulting lift and pitching moment coefficient curves for both wings are presented in Fig. 6a,b together with the experimental data. Similarly, the span-wise lift coefficient distributions are shown in Fig. 6c.

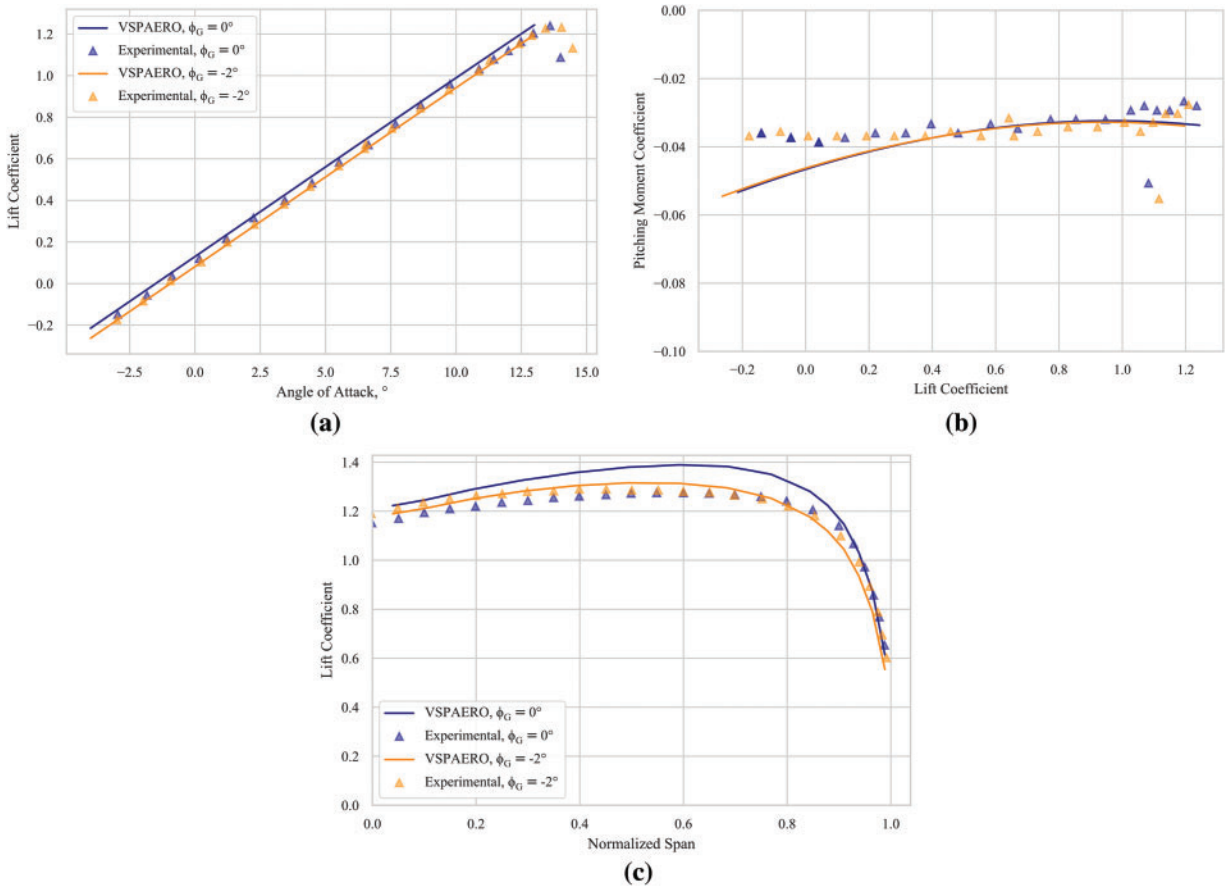

Figure 6: Calculated (a) lift coefficient, (b) pitching moment coefficient, and (c) span-wise lift distribution curves plotted against data points obtained experimentally for the two tested wings at stall

In the same manner as the results of the subsection dealing with the NACA-R1208 wing, the calculated lift curves follow the experimental points remarkably well. The pitching moment coefficient curve loses accuracy at the extremes of the studied range. Finally, the span-wise lift coefficient distribution shows good agreement in both cases. A summary of the obtained values is presented in Table 4. It should be noted that the high percentile error observed in the pitching moment coefficient can be explained by the small value of this parameter; although the absolute error is relatively low.

Table 4: Comparison between the VSPAERO simulation results and the measurements reported in [20]

	Wing 1			Wing 2		
Coefficient	TN-1442	VSPAERO	Error, %	TN-1442	VSPAERO	Error, %
C_{L_α}, rad^{-1}	4.850	4.915	1.34	4.938	4.920	0.38
$\frac{dC_M}{dC_L}$	0.0071	0.0128	81.69	0.0059	0.0121	106.12
$c_L = f\left(\frac{2y}{b}\right)$	—	—	5.82	—	—	2.26

2.6 Low-Re Wings of Different Aspect Ratios

In order to validate the applicability of the solver to wings at low Reynolds number flows, the last two case studies make use of the wind tunnel test results reported in [16] as reference to compare against the calculated values. In the first case study, the lift curves of a set of four rectangular wings with different aspect ratios (AR), shown in Fig. 1f, were calculated considering $Re = 100{,}000$. Further details of this wing family are presented in Fig. A6 and Table A6.

The calculated lift curve plots for the four wings alongside the experimentally determined data points are shown in Fig. 7. From the resulting image it becomes clear that the solver has a tendency to under-predict the lift curve slope for the wings of the smallest aspect ratio. This can be attributed to either viscous or out-of-plane aerodynamic effects (e.g., vortex lift) that are not considered by the VLM solver. The obtained lift curve slope and percent error results are summarized in Table 5 confirming that the wings with smaller aspect ratio present increased deviations while the wings of higher AR show better agreement with the experimental data.

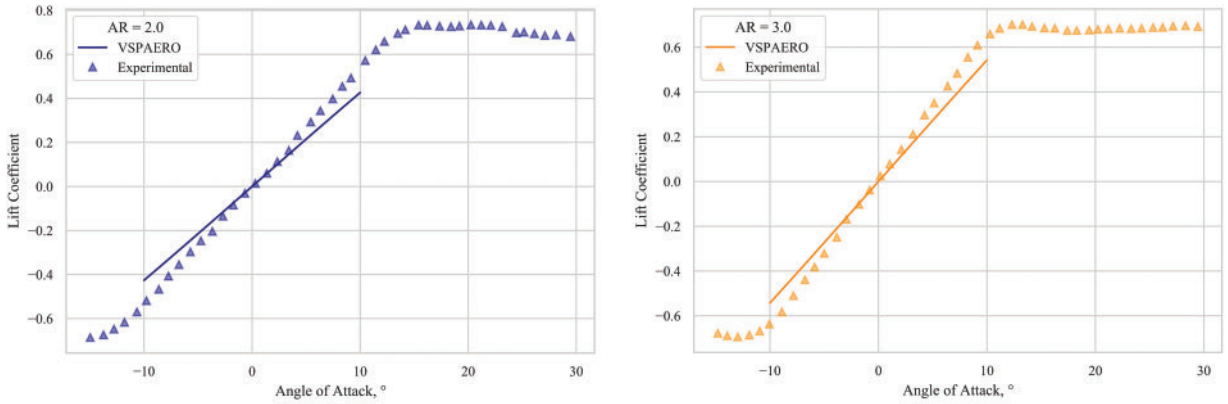

Figure 7: (Continued)

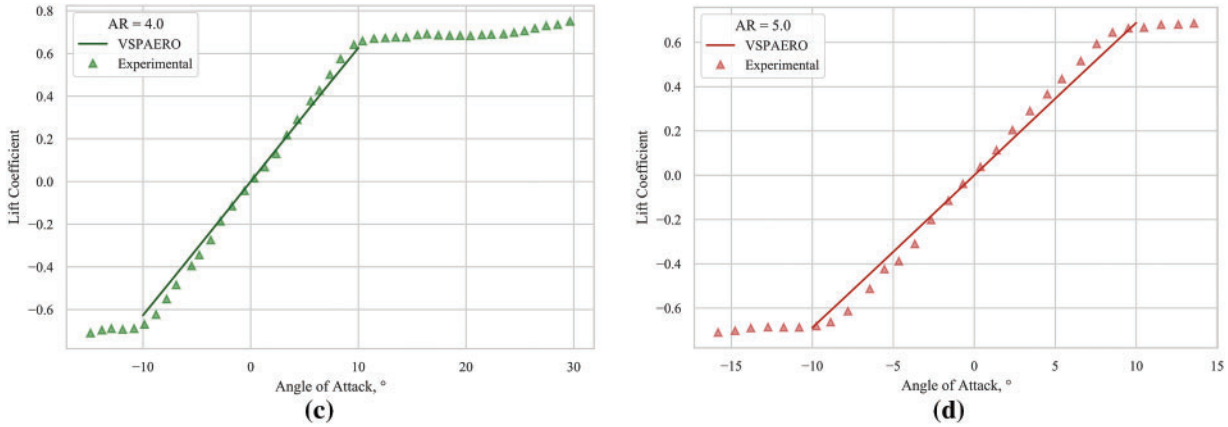

Figure 7: Calculated and experimentally determined lift curves for the following aspect ratios: (a) AR = 2.0, (b) AR = 3.0, (c) AR = 4.0 and (d) AR = 5.0

Table 5: Comparison between the VSPAERO and experimental results for various aspect ratios

Ratio	Experimental, rad^{-1}	VSPAERO, rad^{-1}	Error, %
2.0	3.0814	2.4483	20.55
3.0	3.6697	3.1137	15.15
4.0	3.7876	3.5926	5.15
5.0	3.8615	3.9388	2.00

2.7 Low-Re Wings of Different Taper Ratios

For the last case study, a set of small wings of different taper ratio (TR) (shown in Fig. 1g) operating at $Re = 100{,}000$ are considered. More details of these wings are presented in Fig. A7 and Table A7. Fig. 8 shows the three lift curves calculated using VSPAERO alongside the experimental data points. Similarly to the case of the wings with higher aspect ratio analyzed in the previous section, the calculated lift curves follow the experimental data points in a relatively precise manner. This agreement may be a byproduct of all the studied wings having an aspect ratio of 4.0, the minimum value that yielded good results in the previous validation case. The lift curve slope and error values resulting from the analyses are compiled in Table 6. This table also shows that the resulting error does not seem to follow a trend with regards to the taper ratio.

3 Discussion

The tests carried out showed that chord- and span- wise tessellation values of 33 and 24, respectively, yield acceptable results. This observation was maintained in the remaining case studies. Nonetheless, it should be noted that particular cases may require additional validation.

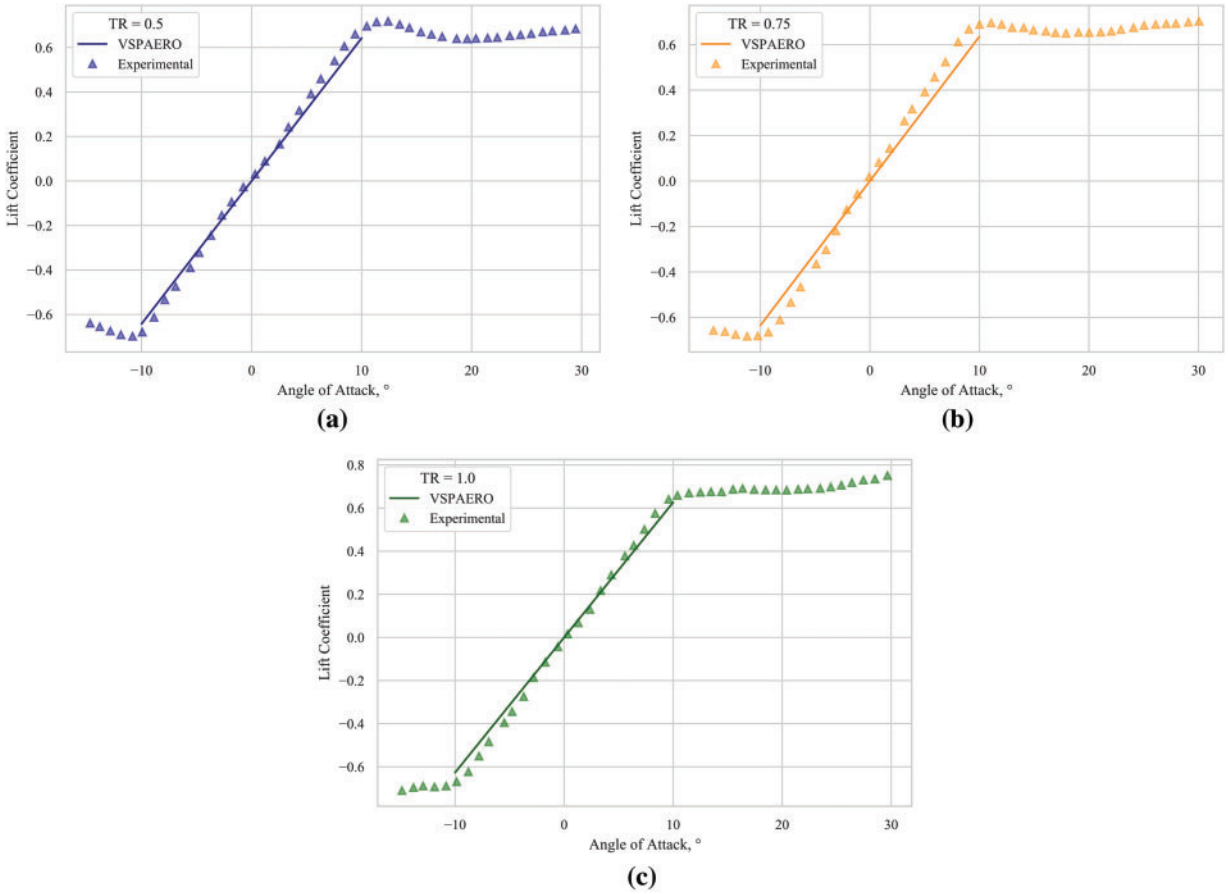

Figure 8: Calculated and experimentally determined lift curves for the following taper ratios: (a) TR = 0.5, (b) TR = 0.75 and (c) TR = 1.0

Table 6: Comparison between the VSPAERO and experimental results for various taper ratios

Ratio	Experimental, rad^{-1}	VSPAERO, rad^{-1}	Error, %
0.5	3.8971	3.6905	5.3
0.75	3.9128	3.6471	6.79
1.00	3.7876	3.5926	5.15

With the exception of the first two wings tested in the previous section, all lift and moment curve slope and distribution calculations provided accurate results well within the ±5% band of the reference values. The fact that this applies for both handbook, theoretical, and experimental values as well as for different flow regimes proves the value of VSPAERO as an aerodynamic prediction tool. Nonetheless, the inherent limitations of the solver should be taken into account, mainly:

- The resulting lift curve is limited to the linear region where viscous characteristics are mostly confined within the boundary layer.

• In highly swept wings an accurate lift prediction may not correspond to an accurate pitching moment calculation.

The linear nature of the solver also imposes some limitations on the wing geometry and flow conditions that may be analyzed accurately, namely:

• The analysis of wings with an aspect ratio less than 4.0 seems to yield overly-pessimistic results when compared with the corresponding reference values, once this minimum aspect ratio is surpassed the percent error margins are significantly reduced.

• The study of highly swept wings, were a span-wise flow component can lead to early tip-stalling, must be kept within a conservative AOA range if good lift and moment predictions are desired.

• Ordinary taper ratio variations did not seem to have a significant effect on the accuracy of the results given that the other geometric considerations are kept in mind.

Finally, Table 7 shows a summary of the suggested settings.

Table 7: Suggested settings

Parameter	Value
Chordwise tessellation	33
Spanwise tessellation	24
AR	>4
Swept wings	Span-wise flow component can lead to early tip-stalling, analyses must be kept within a conservative AOA range if good lift and moment predictions are desired.
AOA range	$-10°$ to $10°$
Ma	<0.3 (i.e., incompressible flow regime)

4 Conclusion

The results obtained from this collection of case study validate the applicability of VSPAERO as an aerodynamic analysis tool for the estimation of, among others, lift and moment characteristics of a typical aircraft wing during the conceptual phase of its development. A more nuanced use of the tool can lead to overall more accurate results, this can be achieved by employing the recommended meshing parameters selection methodology as well as by taking into consideration the reported software limitations related to both wing geometry and flow conditions.

The results obtained from this collection of case studies validate the applicability of VSPAERO as an aerodynamic analysis tool for the estimation of, among others, lift and moment characteristics of a typical lifting surface around its design point during the conceptual phases of an aerial vehicle development. As any other potential flow solver, it is limited to the linear region of the lift curve for accurate predictions and relatively conservative planform geometries. That is, an aspect ratio of at least 4 and as little sweep as possible for good moment coefficient results over a larger angle of attack range; all this under an incompressible flow regime. Nevertheless, as it was demonstrated by the different cases presented in this document, if these limitations are kept in mind while performing the analyses, outstandingly good results can be obtained with relatively little computational time and effort. Moreover, the ability to access, modify and test OpenVSP geometry through scripting APIs

greatly augments the usability of the software package in aircraft development processes, as it enables the possibility of automated optimization design routines from the early stages of the design.

Future work should focus on validating some of the other analysis tools available in VSPAERO. For instance, the aerodynamic-propulsive analysis possibilities and the tools for flight dynamics characterization.

Acknowledgement: Authors wish to acknowledge the PAYCIT-UANL program for their support in this research project.

Funding Statement: The authors received no specific funding for this study.

Author Contributions: The authors confirm contribution to the paper as follows: study conception and design: Jose Rosas-Cordova, Luis Amezquita-Brooks; data collection: Jose Rosas-Cordova; analysis and interpretation of results: Jose Rosas-Cordova, Luis Amezquita-Brooks; draft manuscript preparation: Jose Rosas-Cordova, Luis Amezquita-Brooks, Carlos Santana-Delgado, Diana Hernadez-Alcantara; investigation: Luis Amezquita-Brooks, Diana Hernadez-Alcantara; validation: Carlos Santana-Delgado, Diana Hernadez-Alcantara; resources: Carlos Santana-Delgado, Diana Hernadez-Alcantara. All authors reviewed the results and approved the final version of the manuscript.

Availability of Data and Materials: The data that support the findings of this study are openly available in GitHub at https://github.com/JARC99/vspaero-validation-studies (accessed on 17 September 2024).

Ethics Approval: Not applicable.

Conflicts of Interest: The authors declare that they have no conflicts of interest to report regarding the present study.

References

1. Chandan K, Devi S, Nagaraja KV. Effective evaluation of aerodynamic characteristics using subparameric finite element transformation for unmanned air vehicles at low Reynolds number. Materials Today: Proceedings. 2023 Sep. doi:10.1016/j.matpr.2023.09.197.
2. Okonkwo P, Jemitola P. Integration of the athena vortex lattice aerodynamic analysis software into the multivariate design synthesis of a blended wing body aircraft. Heliyon. 2023 Mar;9(3):e14702. doi:10.1016/j.heliyon.2023.e14702.
3. Shafer T, Viken S, Favaregh N, Zeune C, Williams N, Dansie J. Comparison of computational approaches for rapid aerodynamic assessment of small UAVs. In: Proceedings of the 52nd Aerospace Sciences Meeting, American Institute of Aeronautics and Astronautics (AIAA), 2014 Jan; National Harbor, MD, USA. doi:10.2514/6.2014-0039.
4. Guzelbey I, Eraslann Y, Dogru M. Numerical investigation of different airfoils at low reynolds number in terms of aerodynamic performance of sailplane. Black Sea J Sci. 2018 Jun;8(1):47–65. doi:10.31466/kfbd.423932.
5. National Aeronautics and Space Administration. OpenVSP. 2012. [Online]. Available from: http://openvsp.org. [Accessed 2023 Jul 9].
6. Litherland B. Using VSPAERO. 2015. [Online]. Available from: http://openvsp.org/ wiki/-doku.php?id=vspaerotutorial. [Accessed 2023 Jul 9].
7. Kody F, Bramesfeld G. Small UAV design using an integrated design tool. Int J Micro Air Veh. 2012 Jun;4(2):151–63. doi:10.1260/1756-8293.4.2.151.

8. Bronz M, Hattenberger G, Moschetta J. Development of a long endurance mini-UAV: ETERNITY. Int J Micro Air Veh. 2013 Dec;5(4):261–72.doi:10.1260/1756-8293.5.4.261.
9. Simmons B, McClelland HG, Woolsey C. Nonlinear model identification methodology for small, fixed-wing, unmanned aircraft. J Aircr. 2019 May;56(3):1056–67. doi:10.2514/1.C035160.
10. Cárdenas E, Boschetti P, Amerio A. Stability and flying qualities of an unmanned airplane using the vortex-lattice method. J Aircr. 2009 Jul;46(4):1461–5. doi:10.2514/1.44306.
11. Champasak P, Panagant N, Pholdee N, Vio GA, Bureerat S, Yildiz BS, et al. Aircraft conceptual design using metaheuristic-based reliability optimization. Aerosp Sci Technol. 2022 Oct;129(2):107803. doi:10.1016/j.ast.2022.107803.
12. Champasak P, Panagant N, Pholdee N, Bureerat S, Riza Yildiz A. Self-adaptive many-objective meta-heuristic based on decomposition for many-objective conceptual design of a fixed wing unmanned aerial vehicle. Aerosp Sci Technol. 2020 May;100:105783. doi:10.1016/j.ast.2020.105783.
13. Payne L. VSPAERO verification testing. In: OpenVSP Workshop. San Luis Obispo, CA, USA: Inc.; [Online]. Available from: http://openvsp.org/wiki/lib/exe/fetch.php?media=workshop17:payne-vspaero_verification.pdf. [Accesed 2023 Jul 9].
14. F Mariën, Software testing: VSPAERO (M.S. Thesis). Department of Automotive and Aeronautical Engineering University of Applied Science: Hamburg, Germany; 2021.
15. Great OWL Publishing. SURFACES-User Manual-Vortex-Lattice Module. 2009. [Online]. Available from: http://www.flightlevelengineering.com/downloads/vlm.pdf. [Accessed 2023 Jul 9].
16. Kumar G, Krishnan A. Aerodynamic performance of low-to-moderate aspect ratio wings at low reynolds numbers (M.S. Thesis). The Department of Aerospace Engineering at the University of Illinois Urbana-Champaign: Urbana, IL, USA; 2012.
17. Bertin J, Cummings R. Aerodynamics for engineers. NJ, USA: Pearson; 2013.
18. Schneider W. A comparison of the spanwise loading calculated by various methods with experimental loadings obtained on a 45° sweptback wing of aspect ratio 8.02 at Reynolds 4.0×10^6. NASA, USA: 1951. Report.: 1208.
19. Chen G, Ma D, Jia Y, Xia X, He C. Comprehensive optimization of the unmanned tilt-wing cargo aircraft with distributed propulsors. IEEE Access. 2020 Jul;8:137867–83. doi:10.1109/ACCESS.2020.3012481.
20. Sivells JC. Experimental and calculated characteristics of three wings of NACA 64-210 and 65-210 airfoil sections with and without 2° washout. NASA, USA: 1947. Technical Note No.:1422.
21. Joseph C, Mohan R. A parallel, object-oriented framework for unsteady free-wake analysis of multi-rotor/wing systems. Comput Fluids. 2021 Jan;215(1):104788. doi:10.1016/j.compfluid.2020.104788.

Appendix A

A.1 3D Properties of Two Wings

Table A1 contains a summary of the planform geometry alongside the main simulation parameters employed in the analyses. The two wing geometries employed in the first case study can be seen in Fig. A1.

A.2 Warren-12 Wing

The published planform geometry and aerodynamic characteristics of the wing are compiled in Table A2, the OpenVSP model is shown in Fig. A2.

Table A1: Geometric and simulation parameters employed in the test case study

Parameter	Wing 1	Wing 2
Span	10 ft	10 ft
Chord	1 ft	1 ft
Aspect ratio	10	10
Leading edge sweep	0	35°
Airfoil	NACA 0009	NACA 0009
Angle of attack	10°	10°
Mach number	0.151	0.151
Chord-wise tessellation range	5–133	5–133
Span-wise tessellation range	6–54	6–54

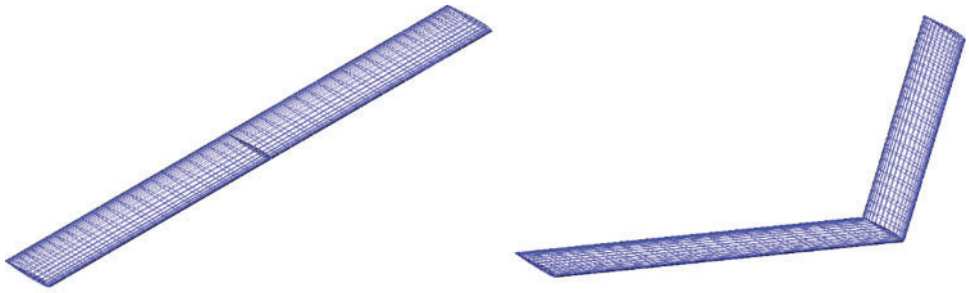

(a) (b)

Figure A1: Wings with (a) 0° and (b) 35° sweep angles used for the validation study

Table A2: Published geometric and aerodynamic characteristics of the Warren-12 wing

Parameter	Value
Span	2.83 ft
Root chord	1.50 ft
Tip chord	0.50 ft
Aspect ratio	2.83
Leading edge sweep	53.54°
C_{L_α} [1]	2.743 rad^{-1}
C_{M_α} [2]	−3.10 rad^{-1}

Note: [1] $c_{ref} = 1$ ft. [2] $x_{CG} = 0$ ft.

A.3 Bertin-Smith 2D Wing

Table A3 summarizes the wing geometry as well as the calculated lift curve slope reported in the book. Fig. A3 shows the wing geometry modelled in OpenVSP.

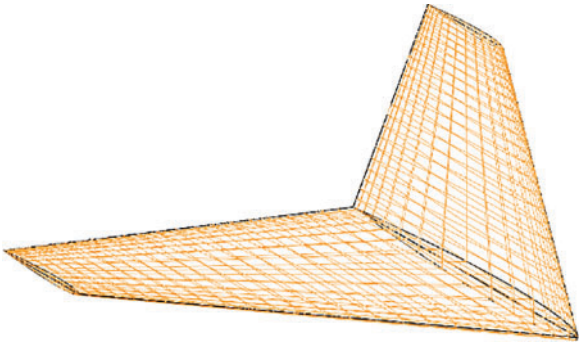

Figure A2: Warren-12 wing modelled in OpenVSP

Table A3: Geometric and aerodynamic characteristics of the Bertin-Smith wing

Parameter	Value
Span	1.0 ft
Chord	0.20 ft
Aspect ratio	5.0
Leading edge sweep	45
C_{L_α} [1]	3.433 rad^{-1}

Note: [1]At $\alpha = 0°$.

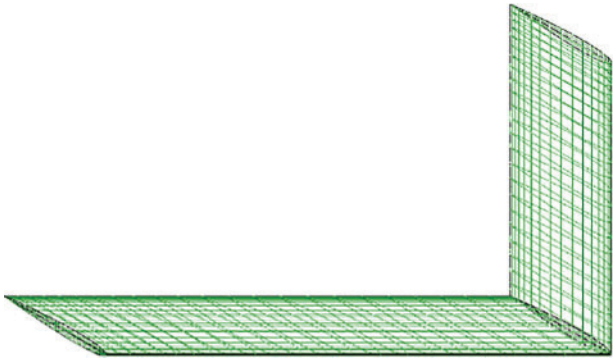

Figure A3: OpenVSP model of the Bertin-Smith wing

A.4 NACA R-1208

The main geometric characteristics of the wing are summarized in Table A4 while the generated OpenVSP geometry is shown in Fig. A4.

A.5 NACA TN-1422

A summary of the planform geometry is presented in Table A5 while the general wing planform is shown in Fig. A5.

Table A4: Geometric parameters of the NACA R-1208 wing studied in [18]

Parameter	Value
Span	10.605 ft
Root chord	1.828 ft
Tip chord	0.823 ft
Aspect ratio	8.0
Quarter chord sweep	45°
Airfoil	NACA 63_1A012

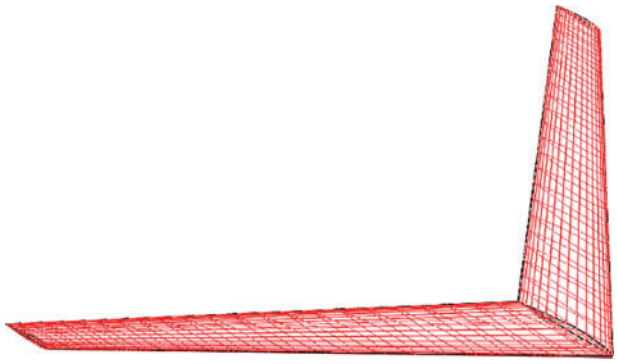

Figure A4: NACA R-1208 wing geometry modelled in OpenVSP

Table A5: Geometric characteristics of the NACA TN-1422 wings tested in [20]

Parameter	Wing 1	Wing 2
Span	15.0 ft	15.0 ft
Root chord	21.381 ft	21.381 ft
Tip chord	0.952 ft	0.952 ft
Aspect ratio	9.0	9.0
Quarter chord sweep	0.0	0.0
Dihedral	3.0	3.0
Washout	0.0	2.0
Airfoil	NACA 65-210	NACA 65-210

A.6 Low-Re Wings of Different Aspect Ratios

Table A6 summarizes the geometry of the analyzed wings while the OpenVSP models of the four studied planforms are shown in Fig. A6.

A.7 Low-Re Wings of Different Taper Ratios

The geometric parameters of the three analyzed wings are compiled in Table A7 while Fig. A7 shows the corresponding OpenVSP models.

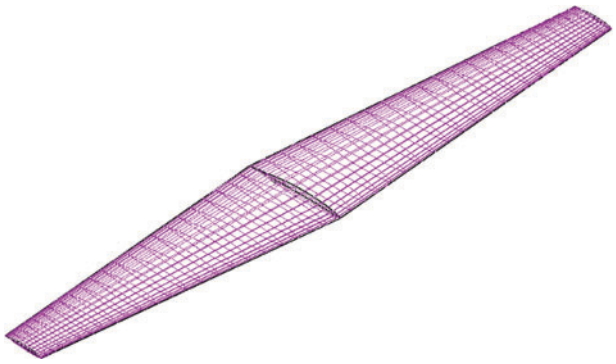

Figure A5: NACA TN-1422 wing geometry modelled in OpenVSP

Table A6: Geometric characteristics of the four low Re tested wings with different AR

Parameter	Wing 1	Wing 2	Wing 3	Wing 4
Span	0.583 ft	0.875 ft	1.167 ft	1.458 ft
Chord	0.292 ft	0.292 ft	0.292 ft	0.292 ft
Aspect ratio	2.0	3.0	4.0	5.0

(a) **(b)** **(c)** **(d)**

Figure A6: Wings with aspect ratio values of (a) 2.0, (b) 3.0, (c) 4.0 and (d) 5.0 modelled in OpenVSP

Table A7: Geometric characteristics of the three low Re tested wings with different taper ratios

Parameter	Wing 1	Wing 2	Wing 3
Span	1.125 ft	1.159 ft	1.167 ft
Root chord	0.375 ft	0.331 ft	0.292 ft
Taper ratio	0.50	0.75	1.00
Aspect ratio	4.0	4.0	4.0

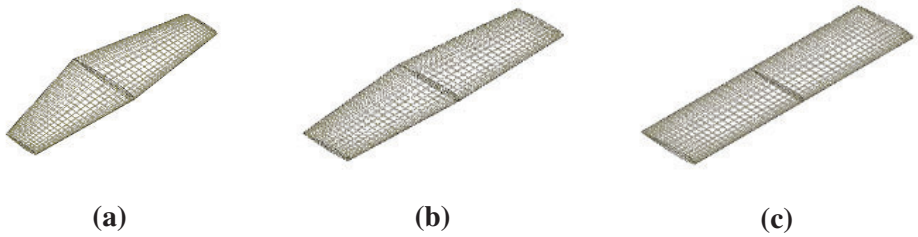

(a) (b) (c)

Figure A7: Wings with taper ratio values of (a) 0.50, (b) 0.75, and (c) 1.00 modelled in OpenVSP